Application of Brillouin thermometry to latest Pleistocene and Holocene halite from Searles Lake, California, USA

Kristian Olson, Emmanuel Guillerm, Mark Peaple, Tim Lowenstein, Véronique Gardien, Frédéric Caupin, Sarah Feakins, Jessica Tierney, Justin Stroup, Steve Lund, et al.

Application of Brillouin thermometry to latest Pleistocene and Holocene halite from Searles Lake, California, USA

Kristian J. Olson [a,*], Emmanuel Guillerm [b,c], Mark D. Peaple [d], Tim K. Lowenstein [a], Véronique Gardien [b], Frédéric Caupin [c], Sarah J. Feakins [d], Jessica E. Tierney [e], Justin Stroup [f], Steve Lund [d], and David McGee [g]

[a] Department of Geological Sciences and Environmental Studies, Binghamton University, Binghamton, New York 13902-6000, USA

[b] Université de Lyon, UCBL, ENSL, CNRS, LGL-TPE, Villeurbanne, F-69622, France

[c] Institut Lumière Matière, Université Claude Bernard Lyon 1, CNRS, Université de Lyon, Villeurbanne, F-69622, France

[d] Department of Earth Sciences, University of Southern California, Los Angeles, CA 90089, USA

[e] Department of Geosciences, University of Arizona, Tucson, AZ 85721, USA

[f] Department of Atmospheric and Geologic Sciences, SUNY Oswego, Oswego, NY 13126, USA

[g] Department of Earth, Atmospheric and Planetary Sciences, Massachusetts Institute of Technology, Cambridge, MA 02139, USA

*Corresponding author

E-mail address: kolson2@binghamton.edu (K.J. Olson).

ABSTRACT

Paleoclimate records from lakes of the southwestern USA have been limited by a lack of independent paleothermometers, resulting in conflicting characterizations of millennial-scale variability in temperature and moisture. Here a novel method called Brillouin thermometry is applied to halite-bearing dry intervals of the late Pleistocene/Holocene (45–0 ka) core record of Searles Lake, California. Temperatures during muddy wetter intervals are available from branched glycerol dialkyl glycerol tetraethers (brGDGTs). Halite from the sediment-water interface records lake bottom temperatures during dry, high salinity periods. Analysis of modern saline lakes of various chemistries, depths, climate zones, and mixing regimes shows that: 1) average bottom water temperature is approximately equal to mean annual air temperature, and 2) annual range of bottom water temperature is inversely proportional to lake depth. Brillouin temperatures for eight halite intervals 30.6 ka to 8.5 ka range from 11.8 ± 3.6 to 22.4 ± 3.2 °C. Bottom water temperature variability indicates paleolake depths of ~10 m during halite precipitation. Temperatures from brGDGTs for mud intervals 44.7 ka to 3.6 ka range from 13.4 ± 2.8 to 23.9 ± 3.0 °C. Comparisons of Brillouin temperatures with predicted equilibrium temperatures of salt crystallization shed light on seasonal processes of evaporite deposition and diagenesis. The multiproxy temperature record of Searles Lake agrees with other regional records at glacial/interglacial timescales but displays a wider degree of millennial-scale variability, with temperatures during the last glacial ranging from 8.3 °C below modern mean annual temperatures to 3.8 °C above.

Keywords: Brillouin thermometry; Fluid inclusions; Evaporites; GDGTs; Searles Lake

1. Introduction

Closed basin lake deposits are important archives of continental paleoclimates (Smoot and Lowenstein, 1991). They accumulate sedimentological, biological, and hydrological data from regional-to-intrabasinal spatial scales and millennial-to-diurnal temporal scales (Feakins et al., 2019; Lowenstein et al., 1999; Olson and Lowenstein, 2021; Sirota et al., 2017). The sensitivity of closed basin lakes to changes in inflow/evaporation make them particularly useful for reconstructing regional responses to climate variability, especially when predicting future drought in water stressed regions such as the southwestern USA (Cook et al., 2021; Pierce et al., 2013; Seager et al., 2007, 2009).

Multiple studies of closed basin lakes in the southwestern USA provided detailed records of millennial-scale hydrologic variability but were limited by a lack of available independent temperature proxies, instead characterizing moisture-temperature relationships by temporal correlations to North Atlantic stadial/interstadial variability (Bacon et al., 2020; Benson, 1999; Benson et al., 2003; Lin et al., 1998; Lund et al., 2021; Phillips et al., 1994; Reheis et al., 2015). But these studies differed over whether warm interstadials were wet or dry (and vice versa), which led to differing interpretations of the mechanisms driving regional paleoclimate variability. Recent advances in lacustrine paleothermometry include clumped isotope thermometry from carbonates (e.g., Santi et al., 2020), coupled glacier-lake models (Quirk et al., 2018), and sensitivity scaling of proxy compilations (Ibarra et al., 2018). Here we offer a new paleotemperature technique suitable for halite formed in hypersaline lakes.

Subsurface deposits at Searles Lake, California USA, are characterized by interbedded muds and salts which document fluctuations in lake level of ~100 to 200 m and water volumes by 30–90 km^3 (Smith, 2009). Wet periods (net inflow > net evaporation) are recorded by mud deposition and salts form during dry periods (net evaporation > net inflow). Halite is the most

soluble mineral in the Searles Lake deposit (Olson and Lowenstein, 2021) and thus marks periods when lake water was most concentrated (i.e., periods of hyperaridity). Here, two independent temperature proxies are used to reconstruct temperatures during dry (salt) periods and wet (mud) periods and therefore clarify the relationship between temperature and moisture within a single depositional setting, without relying on chronologic correlations to North Atlantic events or inferring temperature from other proxy records.

First, a new temperature proxy called Brillouin thermometry (El Mekki-Azouzi et al., 2015) is applied to fluid inclusions in halite from Searles Lake. As halite precipitates, slight imperfections in the propagating crystal produce small voids which entrap microdroplets of brine called fluid inclusions. Such fluid inclusions are primary, discrete, rapidly formed, and exquisitely preserved aliquots of the brine from which the halite crystal precipitated. These fluid inclusions preserve the physical characteristics of the paleobrine which can be used to determine the temperature of the brine at the time of fluid entrapment. The first method developed to use halite inclusions as a paleotemperature proxy, referred to as microthermometry, required nucleating a vapor bubble within the fluid inclusion and then observing the temperature at which the vapor phase homogenized into the liquid phase, called the homogenization temperature (Roberts and Spencer, 1995). Although theoretically sound, the method of homogenization temperatures suffered from analytical problems and failures in reproducibility (e.g., Guillerm et al., 2020; Lowenstein et al., 1998). However, the applicability of halite fluid inclusions as accurate paleothermometers has recently been rejuvenated using Brillouin spectroscopy (Guillerm et al., 2020). This new technique uses the same theoretical principles governing homogenization methods, but without the analytical limitations. Both methods are described in the Supplementary Material.

Next, depositional temperatures from interlayered mud units are derived from bacteria-derived branched glycerol dialkyl glycerol tetraethers (brGDGTs) whose relative abundance of specific brGDGTs has been demonstrated to be influenced by temperature and this is reflected in the methylation index of tetraethers (MBT'_{5Me}) (De Jonge et al., 2014). Global calibrations of lake core top MBT'_{5Me} to mean temperature of months above freezing (r^2 = 0.83, RMSE = 2.9 °C) (Martinez-Sosa et al., 2021) are applied to the brGDGT record from Searles Lake (Peaple et al., 2022). MBT'_{5Me} in hypersaline and alkaline lakes fall off the global calibration temperatures (Martinez-Sosa et al., 2021; Wang et al., 2021), but Peaple et al. (2022) found no correlation with downcore salinity estimates for Searles Lake, while finding plausible temperatures and temperature shifts across key transitions in the mud deposits. Here, we compare Brillouin and brGDGT temperature estimates from salt and mud in a core (SLAPP-SRLS17-1A) taken from Searles Lake. The Brillouin/brGDGT temperature record is then compared with Searles Lake paleobrine temperatures predicted from evaporite mineral equilibria in the same sediment archive (Olson and Lowenstein, 2021). This multiproxy comparison reveals the sensitivity of evaporites to temperature-driven alteration and provides insights on the relationship between salt deposition and seasonal temperature variability in perennial saline lakes.

1.1 Searles Lake evolution & history

Pleistocene–Holocene Searles Lake, California, was a saline-alkaline lake fed by the ancestral Owens River (Fig. 1A). The modern Owens River is primarily fed by runoff along the eastern flank of the Sierra Nevada and since 1913 has been diverted by the Los Angeles Aqueduct, upstream of the now dry Owens Lake (Fig. 1A) (Pretti and Stewart, 2002). During pluvial conditions, the Owens River was the link in a chain of five lakes formed by successive downstream spillover: Owens Lake spilled into China Lake which, in turn, spilled into Searles

Lake. At high lake levels, Searles Lake coalesced with China Lake and spilled into Panamint Lake. Lastly, when Panamint Lake overflowed, it spilled into Lake Manly in Death Valley (Gale, 1914; Smith, 1979; Reheis et al., 2014). Searles Lake likely overflowed during Marine Isotope Stages 2 and 6 but was otherwise the terminus for the Owens River throughout much of the Late Pleistocene (Smith, 2009). Today Searles Lake is a dry saline pan (Fig. 1B).

Fluctuations in inflow and evaporation rates during the Pleistocene and Holocene are loosely characterized by the alternating deposits of salts and muds in Searles Lake (Fig. 1C) (Smith, 2009). Hydrothermal spring flow from Long Valley Caldera (Fig. 1A) in the upper Owens River catchment today contributes 1/3 of the total solutes to the Owens River and accounts for much of the river's bulk chlorinity and alkalinity (Pretti and Stewart, 2002). Evaporation of Owens River water produces a complex suite of chemical sediments including carbonates, sulfates, borates, silicates, and chlorides — in the form of ~25 different minerals (Smith, 1979; Olson and Lowenstein, 2021).

Brine evolution at Searles Lake, driven by evaporation, is characterized by the following mineral sequence (Fig. 2, Olson and Lowenstein, 2021). First, calcite/aragonite [$CaCO_3$] and dolomite [$CaMgCO_3$] precipitate and are deposited along with clastic silt and clay as laminated mud on the lake floor. Upon further evaporative concentration, calcite/aragonite are replaced by displacive crystals of gaylussite [$Na_2Ca(CO_3)_2 \cdot 5H_2O$] or pirssonite [$Na_2Ca(CO_3)_2 \cdot 2H_2O$]. Further evaporation results in precipitation of Na-carbonates (e.g., trona [$Na_2CO_3 \cdot NaHCO_3 \cdot 2H_2O$] or natron [$Na_2CO_3 \cdot 10H_2O$]) and Na-sulfates (e.g., burkeite [$Na_6(CO_3)(SO_4)_2$] or mirabilite [$Na_2SO_4 \cdot 10H_2O$]). These sodium-bearing minerals form at the air-water interface or in the water column and are deposited as "cumulates" on the lake bottom after settling through

the water column. The last mineral to form is halite [NaCl], which precipitates on the lake floor as "bottom growth".

Olson and Lowenstein (2021) found that the predominant saline mineral sequence in the Lower Salt and Upper Salt at Searles Lake is trona → burkeite → halite, which indicates brine temperatures between 20–29 °C during evaporite precipitation. However, these temperature estimates only consider the evaporite record from a thermodynamic perspective, and temperatures for *sequences* of evaporites which likely reflect hundreds of years of deposition. This temperature estimate also does not take into account the conditions under which saline minerals form in mud units, such as gaylussite and pirssonite (Olson and Lowenstein, 2021). Furthermore, the estimated 20–29 °C range during deposition of the Lower Salt and Upper Salt is at the upper end of the 8.2–32.8 °C range of mean monthly temperatures for modern Searles Valley (NOAA National Climatic Data Center). Thermodynamic models show that the solubilities of Na-carbonates and Na-sulfates are temperature-sensitive, especially the low temperature salts natron and mirabilite, both of which are absent in the subsurface of Searles Lake.

Here, the Brillouin method is tested as a novel paleothermometer for times of halite precipitation and brGDGTs are used to independently constrain temperatures during mud deposition. Comparisons between the Brillouin/brGDGT temperatures and the thermodynamic-based evaporite facies are then used to obtain a lake temperature record that covers both wet (mud) high lake levels and dry (salt) low lake levels.

2. Materials and Methods

2.1 Searles Lake sediment core

Sonic drilling was used to recover sediment cores from Searles Lake in January 2017 (Fig. 1B,C). Core SLAPP-SRLS17-1A (35.73715, -117.33029), drilled to 76.7 meters below surface (mbs), records ~200 kyr of lake deposition (Bischoff et al., 1985). A second core, SLAPP-SRLS17-1B (35.73715, -117.33033), was drilled from 21.7 to 38.8 mbs to ensure complete recovery of the Lower Salt. Core description, sampling, and photography were performed in 2017 at the Continental Scientific Drilling (CSD) Facility, University of Minnesota. Chronostratigraphy was established using U/Th disequilibrium dating and BACON age-modeling (Fig. S7) (Stroup et al., 2022). Thin section microscopy was used to identify eight halite layers exhibiting bottom-growth textures, which indicates that 1) the halite is primary and 2) the primary fluid inclusions formed at the sediment-water interface at the bottom of the lake and therefore record lake floor temperatures. Halite crystals were removed from a ~2 cm thick interval of each layer and then cleaved into ~0.5 cm^2 fragments for fluid inclusion analysis.

2.2 Brillouin thermometry

Brillouin thermometry was performed at Université Claude Bernard Lyon 1, Lyon, France. The experimental apparatus is illustrated in Figure S2 and the method briefly outlined here and the Supplementary Material. For a comprehensive overview of the theory and methodology of Brillouin thermometry, see El Mekki-Azouzi et al. (2015), Guillerm (2019), and Guillerm et al. (2020). Halite samples were placed in a temperature-controlled heating-cooling stage (Linkam, Tadworth, UK, THMS600) and observed with a microscope/camera (Zeiss Axioscope) to select and document fluid inclusions which met the size, depth, and isolation criteria outlined by Guillerm et al. (2020). A 4W, 532 nm longitudinal monomode laser beam was generated (Coherent, Verdi V6) and split into a reference beam which bypassed the experimental setup, and an experiment beam. The experiment beam, dimmed to 54 mW, entered

183 the microscope, passed through the objective (Mitutoyo PlanApo, 100x magnification), and
184 focused to a 1 μm spot size on a fluid inclusion. The backscattered light was analyzed with a six-
185 pass tandem Fabry-Pérot interferometer (JRS Scientific, Mettmenstetten, Swiss, TFP-1) to
186 measure the frequency shift of the inelastically scattered light with respect to the reference laser
187 beam. The Brillouin frequency shift (Δf_B) was then used to derive the acoustic velocity of the
188 fluid inclusion and plotted as a function of the temperature of the experiment (Fig. A-1D).
189 Brillouin thermometry was performed on four to nineteen fluid inclusions per ~0.5 cm^2
190 crystal, and two to three crystals per ~2 cm thick halite layer. The acoustic velocity of each fluid
191 inclusion was measured at four temperatures (e.g., 5, 13, 21, 29 °C). Once quasi-isochoric
192 measurements were completed, the sample was heated to 130 °C and then cooled to room
193 temperature in order to cause an irreversible increase in the volume of the inclusions, and thus
194 nucleate a vapor bubble in the fluid inclusions. The acoustic velocity of each, now biphasic, fluid
195 inclusion was measured at four temperatures, which defines the curve along liquid-vapor
196 equilibrium (LVE). A parabolic best-fit of the two sets of four datapoints was used to define the
197 isochore and LVE, respectively. T_x is defined as the point where the two curves intersect (Fig. A-
198 1D).
199 T_x was determined for each individual fluid inclusion measured with an analytic error of
200 ~2 °C (Supplementary Material). The tiny size (3–23 μm) of the fluid inclusions relative to halite
201 precipitation rate (~ cm/yr scale) ensures that each fluid inclusion records a temporally precise
202 'snapshot' of brine temperature. The average T_x for a whole crystal is obtained by calculating the
203 average of the individual fluid inclusion T_x population with standard error calculated using a
204 Student's t-distribution. T_x for a stratigraphic layer was calculated as a weighted average from
205 the mean and SD of the crystals within the layer. T_x is therefore considered at three different

spatiotemporal scales: the fluid inclusion scale, the halite crystal scale, and the halite layer scale. The latter provides the best representative average bottom water temperature, whereas the minimum-maximum difference between the halite crystals within the stratigraphic layer (T_x range) provides insight into the shorter, probably seasonal, temperature variations (Brall et al., 2022).

2.3 GDGT analyses

Ground, dried sediments (~20 g) were extracted using a Dionex Accelerated Solvent Extraction system at the University of Southern California with 9:1 dichloromethane (DCM):methanol (MeOH) at 100 ºC and 1500 psi to yield the total lipid extract (TLE). The TLEs were then separated into neutral and acid fractions using columns packed with NH_2 coated silica gel. Neutral fractions were eluted using 2:1 DCM:isopropanol. The neutral polar fraction was dissolved in hexane:isopropanol (99:1) and filtered through a 0.45 μm PTFE filter prior to analysis by Agilent 1260 High-Performance Liquid Chromatography (HPLC) coupled to an Agilent 6120 mass spectrometer at the University of Arizona. Separation of the brGDGTs was achieved using two BEH HILIC silica columns (2.1 mm × 150 mm, 1.7 μm; Waters) following the methods of Hopmans et al. (2016). The relative methylation of the 5′ isomers of the brGDGTs is expressed as the MBT'_{5Me} index (De Jonge et al., 2014).

$$MBT'_{5Me} = (Ia + Ib + Ic)/(Ia + Ib + Ic + IIa + IIb + IIc + IIIa) \quad (1)$$

Duplicate analyses as well as analyses of an internal laboratory standard throughout the runs yielded an error of 0.009 MBT'_{5Me} units (1σ). A 200 kyr record of brGDGT temperatures for Searles lake are reported by Peaple et al. (2022). In that study, Searles Lake brGDGTs distributions are compared with the distribution of brGDGTs from global lake and soil datasets and they find that a lake calibration is most appropriate. We therefore convert MBT'_{5Me} into

mean temperature of Months Above Freezing (MAF) using a Bayesian global lake calibration $BayMBT_0$ (Martínez-Sosa et al., 2021) with reported calibration RMSE of 2.9 °C (n = 65, R^2 = 0.82).

2.4 Modern analogs

Meaningful interpretation of Pleistocene Searles Lake bottom water temperatures requires knowledge of the relationship between the air, surface water, and bottom water temperatures of modern saline lakes. These relationships are first established for Great Salt Lake, Utah, using the Great Salt Lake chemical database which is maintained by the Utah Geologic Survey and contains high-resolution lake temperature data from 1966 to 2014 (Rupke and McDonald, 2012). Great Salt Lake is an appropriate analog for reconstructing temperatures at Searles Lake due to the large seasonal variability in temperature as well as its periodic supersaturation with respect to mirabilite and halite. Nonetheless, saline lakes are unique with respect to chemistry, stratification, hypsometry, volume, surface area, and geography. As such, any prudent application of a modern lake as an analog for an ancient system requires multiple analogs, where available, to increase confidence that an observed behavior is characteristic of saline systems in general. For this reason, additional data from nine non-tropical saline lakes of various depths and salinities are used to confirm the relationships observed in Great Salt Lake (Supplementary Material).

3. Results

Brillouin thermometry is applied to four layers from the Upper Salt (15.6–0 ka) and four layers from the Lower Salt (38.5–22.6 ka). All the halite samples are separated by muds (Lower Salt) or non-halite evaporites (Upper Salt), except for two samples from the S7 unit of the Lower Salt. The fluid inclusions analyzed in multiple crystals from each layer were used to determine a

bottom water temperature for each crystal, and the maximum, minimum and mean bottom water temperature for each layer (Table 1). For the Upper Salt, mean bottom water temperatures vary from 19.4 ± 2.6 to 22.4 ± 3.2 °C with ranges of 3.0 to 7.8 °C. The Lower Salt yields a mean of 11.8 ± 3.6 to 19.1 ± 1.8 °C and range of 4.6 to 10.8 °C. Estimating depositional rates of evaporites is difficult given 1) the bimodal crystallization rates for cumulates and bottom growth and 2) the sensitivity of crystallization rates to changes in temperature, evaporation, and ionic composition. The age model indicates accumulation of 0.16 cm/yr for the S7 halite unit (Stroup et al., 2022), or 13 years for 2 cm. However, halite deposition rates are typically much faster in modern systems (e.g., Dead Sea, 10 cm/yr, Lensky et al., 2005), indicating that alternating muds are slowing the apparent accumulation rate in S7 and 2 cm of halite crystals could represent <1 yr.

Unlike Brillouin thermometry on selected crystals in the halite layers, brGDGT thermometry can be continuously applied across the mud units (including the Parting Mud, Bottom Mud, and M6) to yield a timeseries from which variability can be assessed. BrGDGT temperature estimates range from 13.4 ± 2.8 °C to 23.9 ± 3.0 °C, with an average of 18.7 ± 2.8 °C from 45–0 ka (Table 2). The average depositional rate for the Parting Mud is 0.05 cm/yr (Stroup et al., 2022), so brGDGTs extracted from 2 cm samples integrate ~ 40 years.

4. Discussion

4.1 From temperature to lake depth

To ascertain the climatic significance of the Brillouin thermometric data from Searles Lake halite, a relationship must be established between the temperatures on the lake floor where halite crystals grow and mean annual or seasonal air temperatures. Additionally, the variable(s)

276 controlling annual fluctuations in bottom water temperature must be determined, as well as the
277 relationship between the average temperatures and the temperature ranges.

278 The thermal structure, mixing, and bottom water temperatures of freshwater lakes are
279 largely determined by regional climate-controlled temperatures and the maximum density of
280 water (1 g/cm^3) at 3.98 °C (Hutchinson and Löffler, 1956). For example, if autumn cooling
281 lowers surface waters to ~4 °C, then a density inversion is established which produces downward
282 displacement of denser water and mixing of the water column. During summer, warming and
283 expansion of surface water creates vertical density stratification where the densest water remains
284 at ~4 °C at the bottom of the lake. Generally, deep , non-tropical, freshwater lakes maintain 4 °C
285 bottom water temperatures year-round (Butcher et al., 2015), and are therefore insensitive to
286 mean annual air temperatures (MAAT).

287 Unlike freshwater lakes, the behavior of saline lakes is not constrained by the ~4 °C
288 density maximum of water, as brine densities are considerably higher due to the dissolved salt.
289 Furthermore, the change in density with temperature of saline lakes is much higher than their
290 freshwater counterparts, which contributes to their increased stability (Ferris and Burton, 1988).
291 Saline lakes in non-tropical climates may therefore behave like freshwater tropical lakes, where
292 thermal structures and bottom water temperatures reflect seasonal and annual air temperatures.
293 Nevertheless, the general relationship between saline lake floor temperatures and climate is
294 poorly established, and thus interpretations of temperature data from fluid inclusions in halite
295 precipitated on the floor of ancient Searles Lake first requires investigation of modern saline
296 lakes.

297 The Great Salt Lake region experienced abnormally high precipitation from 1982–1984,
298 which, combined with large snowpack during the winter of 1985, produced a 3.72 m rise of lake

level by 1987 to the historical record of 1283.77 m (Fig. 3A) (Stephens, 1990). Increased freshwater inflow to Great Salt Lake retarded annual overturn (holomixis) and maintained stable meromixis (permanent stratification) until lake level dropped in the 1990s (Fig. 3B). As the depth of Great Salt Lake increased (Fig. 3B), the range of bottom water temperatures narrowed and converged on the mean annual air temperature (Fig. 3C), showing that 1) the annual range of bottom water temperatures is anti-correlated to lake depth (Fig. 3D) and 2) the average bottom water temperature is climatically significant as it reflects MAAT. For Great Salt Lake, bottom water temperature is constant and equal to MAAT of ~10 °C when lake depths are ≥ 12 m (Fig. 3E).

Data for nine non-tropical saline lakes of various depths and salinities confirm the Great Salt Lake observations, as they show a strong correlation ($r = 0.97$) between mean annual air temperatures and average bottom water temperatures, including shallow (< 10 m-deep) saline lakes (Fig. 4A). This correlation means that even if bottom water temperatures are not constant, they still oscillate seasonally around mean annual air temperatures and support the interpretation that layer-averaged Brillouin temperatures from Searles Lake halites record MAAT.

A consistent relationship exists between lake depth and bottom water temperature range for all saline lakes (Fig.4B). The range of bottom water temperatures decreases with depth to ~12–22 m and remains relatively constant (< 2°C variability) at greater depths. This lake depth-temperature relationship is likely due to the combined effects of limited light penetration, wave base, and density stratification and as such is expected to vary between lakes. Here, the linear regression in Figure 4B is used for an upper estimate of Searles Lake depths, and the relationship for Great Salt Lake (Fig. 3E) is used for a lower estimate. Based on the range of temperatures determined within individual halite layers, calculated paleo-depths for Pleistocene/Holocene Searles Lake

during times of halite precipitation ranged from 10.1 to 22.0 m (Table 1). The range of paleodepths captures the range of empirical data for modern saline lakes. Brillouin measurements for Searles Lake halite units provide a *minimum* annual bottom water temperature range, and therefore a *maximum* lake depth estimate. Additionally, the deeper (22.0 m) estimates are derived from modern lakes with low salinity (relative to Great Salt Lake) and are likely less stable (greater bottom water temperature variability) than if they were halite-saturated. For these reasons, the shallower depth estimates of ~10 m are more likely representative of a halite-saturated Searles Lake. Smith (2009) used basin hypsometry and stratigraphic masses to calculate a 0–12 m depth for a halite saturated Searles Lake. Our findings therefore overlap with previous estimates but suggest that the deeper of Smith's (2009) 0-12 m estimate is more likely. A deeper, perennial Searles Lake was also argued by Olson and Lowenstein (2021) as necessary to account for long-term ion inheritance and Searles Lake mass-balance.

4.2 Brillouin/brGDGT versus thermodynamic models

A comparison of Brillouin and brGDGT temperature reconstructions from the Searles Lake core from 40–5 m is shown in Figure 5C. For the most part, interlayered salts (fluid inclusions) and muds (brGDGTs) record similar temperatures, within the uncertainties of each proxy. Both proxies also record similar temperature ranges and temporal trends: the average reconstructed temperature is 17.5 ± 4.1 °C for Brillouin and 18.7 ± 2.8 °C for brGDGTs, with temperature ranges of 10.6 ± 6.8 °C for Brillouin and 10.5 ± 5.8 °C for brGDGTs. For the Holocene, average reconstructed temperatures are 21.1 ± 2.1 °C from Brillouin and 19.8 ± 2.2 °C from brGDGTs, similar to the modern mean annual temperature at Searles Lake, of 20.1 °C.

A temperature record for Searles Lake can also be reconstructed from the assemblages and sequences of evaporite minerals (Olson and Lowenstein, 2021). Trona and burkeite, for

instance, are thermodynamically stable only at temperatures above 15 °C, below which natron and mirabilite precipitate (Fig. 2). The common occurrence of trona and burkeite in the Lower Salt and Upper Salt (Figure 5B), and the lack of natron and mirabilite, thus implies brine temperatures ≥ 15 °C during evaporite deposition. An upper limit for brine temperature (29 °C) is also constrained by evaporite minerals. Above 29 °C, burkeite precipitates prior to trona, but this sequence is never observed in the Searles Lake deposit. While the temperature thresholds are highly dependent on brine chemistry and pCO_2, both are well constrained by the evaporite record (Supplementary Material).

For the Upper Salt (15.6–0 ka), Brillouin and brGDGT temperatures are consistent with the 15–29 °C temperature estimates from the phase assemblages and sequences, and the three temperature proxies are in good agreement. However, Brillouin temperatures for the S4 unit of the Lower Salt are 11.8 ± 3.6 °C, indicating that the Na-carbonate and Na-sulfate phases within that unit should consist of natron and mirabilite instead of trona and burkeite (Fig. 2,5). Brillouin and brGDGT temperatures below 15 °C occur in other intervals of the Lower Salt (38.5–22.6 ka) (e.g., M2–5; S7), indicating natron and mirabilite should also occur in these units. In contrast, the Na-carbonates and Na-sulfates of the Lower Salt are chiefly composed of trona and burkeite, which form above 15 °C. Based on these observations, salts formed in the warm season are preferentially preserved in the Searles Lake deposit. We conclude that the preservation of evaporite deposits is sensitive to seasonal changes in brine temperature, especially low temperature salts such as mirabilite and natron, which form at the lake surface in winter but commonly dissolve in warmer bottom waters.

4.4 Temperature record of Searles Lake

Here, Searles Lake Brillouin and brGDGT temperatures are combined into a 45 kyr paleotemperature record (Table 2) and compared to other regional temperature records. During the last glacial (45–14 ka), Searles Lake was perennial (i.e., never desiccated) and experienced dramatic hydrologic variability as indicated by alternating deposition of salts and muds. Searles Lake temperatures during the last glacial were ~ 2.2 °C lower than today (17.9 ± 3.1 °C) but highly variable, with temperatures ranging from 8.3 °C below to 3.8 °C above mean annual air temperature (MAAT) (Table 2) . During the Last Glacial Maximum (LGM- 23–19 ka), Searles was 2.0 °C lower than today which was followed by deglacial warming of 2.0 °C from 19 ka to 11 ka. Holocene (11–0 ka) temperatures of Searles Lake (20.2 °C) are indistinguishable from modern values (20.1 °C) and exhibit greater stability — fluctuating by only -2.1 °C to +2.8 °C relative to MAAT. The Holocene has been as a prolonged dry period at Searles, with low lake levels and extensive evaporite deposition.

At glacial/interglacial timescales, the Searles Lake temperature proxies agree with regional archives, recording colder/wetter conditions during the last glacial (45–14 ka), temperatures rising to modern values during the deglacial (19–11 ka), and warm/dry conditions during the Holocene. Regional groundwater temperatures during the last glacial were 6.2 ± 0.6 °C lower than today in the San Diego area and 4.2 ± 1.1 °C below modern in the Mojave Desert (Fig. 6B) (Kulongoski et al., 2009; Seltzer et al., 2019). During the LGM, SST along the California margin was ~ 4 °C cooler than today (Herbert et al., 2001). In the Sierra Nevada, the Tioga Glaciation (27–15 ka) reached a maximum snowline depression (ELA) of 1200 m (Phillips, 2017), which corresponds to ~5–6 °C lower MAAT than today (Plummer, 2002). The effects of advancing and retreating Sierra Nevada glaciers are observed in nearby lake records by variations in pollen. Juniper pollen from Owens Lake core OL-92, for example, indicates a 500–

600 m downslope expansion of pinyon-juniper woodland as glaciers advanced and temperatures decreased between 25 ka and 20 ka (LGM). This was followed by a sharp decline in Juniper pollen during deglaciation (19–11 ka; Fig. 6D) (Woolfenden, 2003). A regional hydroclimate record for the western United States was computed from a large dataset of plant macrofossils (packrat middens) (Fig. 6C) (Harbert and Nixon, 2018). A perfect correlation is not expected given the large geographical area (Supplementary Material). But the macrofossil temperature trend during the last glacial is in general agreement with Searles Lake temperatures, including consistently low mean annual temperatures (MATs) during the last glacial, 45–15 ka, warming trend during deglaciation, and maximum MATs in the Holocene (Fig. 6C).

At millennial timescales, Searles Lake sediments record large swings in terrestrial temperatures during the last glacial (45–14 ka), with Brillouin and brGDGTs indicating variability of 12.1 °C. Comparable millennial-scale variability is seen in Lake Elsinore where the pre-LGM (33–23 ka) brGDGT record shows variability of 12.6 °C (Fig. 6E) (Feakins et al., 2019). Searles Lake temperatures vary by 11.1 °C during the same period (Fig. 6A). In contrast, California margin SSTs fluctuated by only 1.1 °C from 33–23 ka (Herbert et al., 2001) and regional groundwaters varied by only 2.5 °C (Fig. 6B) (Kulongoski et al., 2009; Seltzer et al., 2019). This comparison corroborates that large thermal reservoirs, such as groundwater and the ocean, do not respond to millennial scale climate change with the same sensitivity as lakes. During the Holocene, temperature ranges narrow to 4.9 °C for Searles Lake and 6.9 °C for Lake Elsinore.

5. Conclusions

- Brillouin thermometry on fluid inclusions in halite yields temperatures of bottom brines during periods of evaporite deposition in Searles Lake, California, from 45–0 ka.
- The reconstruction of temperatures using the brGDGT thermometer from mud samples reflects mean months above freezing, and corroborates the Brillouin reconstructions of temperature.
- The two techniques measure different materials and facies, which provides a reconstruction of temperature across changing depositional environments in Pleistocene Searles Lake.
- Brillouin thermometry yields a record of bottom water conditions. The mean annual bottom water temperature (MABWT) of non-tropical saline lakes is a proxy for mean annual air temperature (MAAT), whereas the annual range in bottom water temperatures is a proxy for lake depth. For salt saturated lakes, this allows reconstruction of temperature records during lake low-stands, an important compliment to more common high-stand records.
- Between 45 ka to 2.8 ka, when Searles Lake was at halite saturation, the brine was ~10 m deep. Such depths produce two temperature regimes: variable surface temperatures and near-constant bottom brine temperatures. In saline-alkaline lakes, low temperature- salts may precipitate in cold surface waters and then settle to warmer bottom waters where they dissolve, resulting in a temperature-biased evaporite record. Paleotemperature reconstructions based on evaporite phase equilibria should therefore be evaluated with independent proxies such as Brillouin thermometry or brGDGTs.
- This study introduces a paired proxy approach to study temperature across changing facies in perennial lakes with evaporite-mud alterations. The two proxies incorporate low

and high salinity facies to reconstruct temperatures and hydroclimate. The new Searles Lake temperature reconstructions indicate colder conditions during the last glacial, deglacial warming to modern temperatures, and warm conditions during the Holocene. At millennial timescales, Searles Lake dual proxy reconstruction indicates significant temperature variability during the last glacial, with temperatures ranging from 8.3 °C lower than modern to 3.8 °C higher.

DATA AVAILIBILITY

The data associated with this article are archived at the NOAA paleoclimate database. https://www.ncei.noaa.gov/access/paleo-search/study/36836

ACKNOWLEDGEMENTS

We thank Jade Brush and Searles Valley Minerals Inc. for access and support during recovery of core SLAPP-SRLS17. Sample material used in this project was provided by the Continental Scientific Drilling (CSD) Facility, University of Minnesota. This material is based upon research supported by the Chateaubriand Fellowship of the Office for Science & Technology of the Embassy of France in the United States to KO, the Comer Family Foundation funding to TL and DM, US National Science Foundation Award NSF-EAR-1903659, 1903665, 1903519, and 1903544 respectively to TL, SF, JS, and DM, with additional support from GSA, AAPG, and SEG graduate student grants to KO. Part of this work was performed within the framework of the EUR H2O'Lyon (ANR-17-EURE-0018) of Université de Lyon (UdL), within the program "Investissements d'Avenir" operated by the French National Research Agency (ANR). We thank

Patrick Murphy for assistance with GDGT analyses at U. Arizona, supported by Packard Foundation funding to JT.

REFERENCES

Bacon, S.N., Jayko, A.S., Owen, L.A., Lindvall, S.C., Rhodes, E.J., Schumer, R.A., Decker, D.L., 2020. A 50,000-year record of lake-level variations and overflow from Owens Lake, eastern California, USA. Quaternary Science Reviews 238, 106312. https://doi.org/10.1016/j.quascirev.2020.106312

Benson, L., 1999. Records of millennial-scale climate change from the Great Basin of the Western United States, in: Clark, U., Webb, S., Keigwin, D. (Eds.), Geophysical Monograph Series. American Geophysical Union, Washington, D. C., 203–225. https://doi.org/10.1029/GM112p0203

Benson, L., Lund, S., Negrini, R., Linsley, B., Zic, M, 2003. Response of North American Great Basin lakes to Dansgaard–Oeschger oscillations. Quaternary Science Reviews 22, 2239–2251. https://doi.org/10.1016/S0277-3791(03)00210-5

Bischoff, J.L., Rosenbauer, R.J., Smith, G.I., 1985. Uranium-series dating of sediments from Searles Lake: Differences between Continental and Marine climate records. Science 1222–1224. https://doi.org/10.1126/science.227.4691.1222

Brall, N.S., Gardien, V., Ariztegui, D., Sorrel, P., Guillerm, E., Caupin, F., 2022. Reconstructing lake bottom water temperatures and their seasonal variability in the Dead Sea Basin during MIS5e. Depositional Record. Accepted Author Manuscript. https://doi.org/10.1002/dep2.185

Butcher, J.B., Nover, D., Johnson, T.E., Clark, C.M., 2015. Sensitivity of lake thermal and mixing dynamics to climate change. Climatic Change 129, 295–305. https://doi.org/10.1007/s10584-015-1326-1

Cook, B.I., Mankin, J.S., Williams, A.P., Marvel, K.D., Smerdon, J.E., Liu, H., 2021. Uncertainties, limits, and benefits of climate change mitigation for soil moisture drought in southwestern North America. Earth's Future, 9, p.e2021EF002014. https://doi.org/10.1029/2021EF002014

De Jonge, C., Hopmans, E.C., Zell, C.I., Kim, J.H., Schouten, S., Sinninghe Damsté, J.S., 2014. Occurrence and abundance of 6-methyl branched glycerol dialkyl glycerol tetraethers in soils: Implications for palaeoclimate reconstruction. Geochimica et Cosmochimica Acta 141, 97–112. https://doi.org/10.1016/j.gca.2014.06.013

El Mekki-Azouzi, M.E., Tripathi, C.S.P., Pallares, G., Gardien, V., Caupin, F., 2015. Brillouin spectroscopy of fluid inclusions proposed as a paleothermometer for subsurface rocks. Scientific Reports 5, 9. https://doi.org/10.1038/srep13168

Feakins, S.J., Wu, M.S., Ponton, C., Tierney, J.E., 2019. Biomarkers reveal abrupt switches in hydroclimate during the last glacial in southern California. Earth and Planetary Science Letters 515, 164–172. https://doi.org/10.1016/j.epsl.2019.03.024

Ferris, J.M., Burton, H.R., 1988. The annual cycle of heat content and mechanical stability of hypersaline Deep Lake, Vestfold Hills, Antarctica. Hydrobiologia 165, 115–128. https://doi.org/10.1007/BF00025579

Gale, H.S., 1914. Salines in the Owens, Searles, and Panamint basins, southeastern California. U.S. Geological Survey Bulletin 580–L, 251–323. https://doi.org/10.3133/b580L

Guillerm, E., 2019. Turning halite fluid inclusions into accurate paleothermometers with Brillouin spectroscopy [Ph.D. thesis]. Université Claude Bernard Lyon 1, Lyon, France, 229. https://www.theses.fr/2019LYSE1284

Guillerm, E., Gardien, V., Ariztegui, D., Caupin, F., 2020. Restoring Halite Fluid Inclusions as an Accurate Palaeothermometer: Brillouin Thermometry Versus Microthermometry. Geostandards and Geoanalytic Research 44, 243–264. https://doi.org/10.1111/ggr.12312

Harbert, R.S., Nixon, K.C., 2018. Quantitative Late Quaternary climate reconstruction from plant macrofossil communities in western North America. Open Quaternary, 4. 1–13. http://doi.org/10.5334/oq.46

525 Herbert, T.D., 2001. Collapse of the California Current During Glacial Maxima Linked to
526 Climate Change on Land. Science 293, 71–76. https://doi.org/10.1126/science.1059209
527
528 Hopmans, E.C., Schouten, S., Sinninghe Damsté, J.S., 2016. The effect of improved
529 chromatography on GDGT-based palaeoproxies. Organic Geochemistry 93, 1–6.
530 https://doi.org/10.1016/j.orggeochem.2015.12.006
531
532 Hudson, A.M., Hatchett, B.J., Quade, J., Boyle, D.P., Bassett, S.D., Ali, G., De los Santos, M.G.,
533 2019. North-south dipole in winter hydroclimate in the western United States during the
534 last deglaciation. Sci Rep 9, 4826. https://doi.org/10.1038/s41598-019-41197-y
535
536 Hutchinson, G.E., Löffler , H., 1956. The thermal classification of lakes. Proceedings of the
537 National Academy of Sciences of the United States of America 42, 84.
538 https://doi.org/10.1073/pnas.42.2.84
539
540 Ibarra, D.E., Oster, J.L., Winnick, M.J., Caves Rugenstein, J.K., Byrne, M.P., Chamberlain, C.P.,
541 2018. Warm and cold wet states in the western United States during the Pliocene–
542 Pleistocene. Geology, 46, 355–358. https://doi.org/10.1130/G39962.1
543
544 Kulongoski, J.T., Hilton, D.R., Izbicki, J.A., Belitz, K., 2009. Evidence for prolonged El Nino-
545 like conditions in the Pacific during the Late Pleistocene: a 43ka noble gas record from
546 California groundwaters. Quaternary Science Reviews 28, 2465–2473.
547 https://doi.org/10.1016/j.quascirev.2009.05.008

Lensky, N.G., Dvorkin, Y., Lyakhovsky, V., Gertman, I., Gavrieli, I., 2005. Water, salt, and energy balances of the Dead Sea. Water Resources Research 41, W12418. https://doi.org/10.1029/2005WR004084

Lin, J.C., Broecker, W.S., Hemming, S.R., 1998. A reassessment of U-Th and 14C ages for lat-glacial high-frequency hydrological events at Searles Lake, California 49, 11–23. https://doi.org/10.1006/qres.1997.1949

Lowenstein, T.K., Li, J., Brown, C., 1998. Paleotemperatures from fluid inclusions in halite: method verification and a 100,000 year paleotemperature record, Death Valley, CA. Chemical Geology 150, 223–245. https://doi.org/10.1016/S0009-2541(98)00061-8

Lowenstein, T.K., Li, J., Brown, C., Roberts, S.M., Ku, T.-L., Luo, S., Yang, W., 1999. 200 ky paleoclimate record from Death Valley salt core. Geology 27, 3–6. https://doi.org/10.1130/0091-7613(1999)027%3C0003:KYPRFD%3E2.3.CO;2

Lund, S., Benson, L., Negrini, R., 2021. Timing of Sierra Nevadan stadial/interstadial variations from 15 to 56 ka. Quaternary International 583, 31–38. https://doi.org/10.1016/j.quaint.2021.02.007

Martínez-Sosa, P., Tierney, J.E., Stefanescu, I.C., Dearing Crampton-Flood, E., Shuman, B.N., Routson, C., 2021. A global Bayesian temperature calibration for lacustrine brGDGTs.

Geochimica et Cosmochimica Acta 305, 87–105. https://doi.org/10.1016/j.gca.2021.04.038

McGee, D., Moreno-Chamarro, E., Marshall, J., Galbraith, E.D., 2018. Western U.S. lake expansions during Heinrich stadials linked to Pacific Hadley circulation. Science Advances 4, eaav0118. https://doi.org/10.1126/sciadv.aav0118

Meerbeeck, C.J.V., Renssen, H., Roche, D.M., 2009. How did Marine Isotope Stage 3 and Last Glacial Maximum climates differ? – Perspectives from equilibrium simulations. Climate of the Past 5, 33–51. https://doi.org/10.5194/cp-5-33-2009

Olson, K.J., Lowenstein, T.K., 2021. Searles Lake evaporite sequences: Indicators of late Pleistocene/Holocene lake temperatures, brine evolution, and pCO_2. Geological Society of America Bulletin. https://doi.org/10.1130/B35857.1

Peaple, M.D., Bhattacharya, T., Lowenstein, T., McGee, D., Olson, K., Stroup, J.S., Tierney, J.E., Feakins, S.J., 2022. Biomarker and pollen evidence for late Pleistocene pluvials in the Mojave Desert. Earth and Space Science Open Archive, 45. https://doi.org/10.1002/essoar.10511222.1

Phillips, F., 2017. Glacial chronology of the Sierra Nevada, California, from the Last Glacial Maximum to the Holocene. Cuadernos de Investigación Geográfica 43, 527. https://doi.org/10.18172/cig.3233

Phillips, F.M., Campbell, A.R., Smith, G.I., Bischoff, J.L., 1994. Interstadial climatic cycles: A link between western North America and Greenland?. Geology 22, 1115–1118. https://doi.org/10.1130/0091-7613(1994)022<1115:ICCALB>2.3.CO;2

Pierce, D.W., Cayan, D.R., Das, T., Maurer, E.P., Miller, N.L., Bao, Y., Kanamitsu, M., Yoshimura, K., Snyder, M.A., Sloan, L.C., Franco, G., 2013. The key role of heavy precipitation events in climate model disagreements of future annual precipitation changes in California. Journal of Climate, 26, 5879–5896. https://doi.org/10.1175/JCLI-D-12-00766.1

Plummer, M.A., 2002. Paleoclimatic conditions during the Last Deglaciation inferred from combined analysis of pluvial and glacial records [Ph.D. thesis]. New Mexico Institute of Mining and Technology, Socorro, New Mexico, 308. https://www.nmt.edu/academics/ees/theses/theses_1936-2014/2002d_plummer_ma.pdf

Pretti, V.A., Stewart, B.W., 2002. Solute sources and chemical weathering in the Owens Lake watershed, eastern California: Solute sources and chemical weathering. Water Resources Research 38, 2-1–2-18. https://doi.org/10.1029/2001WR000370

Quirk, B.J., Moore, J.R., Laabs, B.J., Caffee, M.W., Plummer, M.A., 2018. Termination II, last glacial maximum, and lateglacial chronologies and paleoclimate from Big Cottonwood

Canyon, Wasatch Mountains, Utah. GSA Bulletin, 130, 1889–1902. https://doi.org/10.1130/B31967.1

Reheis, M.C., Adams, K.D., Oviatt, C.G., Bacon, S.N., 2014. Pluvial lakes in the Great Basin of the western United States—a view from the outcrop. Quaternary Science Reviews 97, 33–57. https://doi.org/10.1016/j.quascirev.2014.04.012

Reheis, M.C., Miller, D.M., McGeehin, J.P., Redwine, J.R., Oviatt, C.G., Bright, J., 2015. Directly dated MIS 3 Lake-Level Record from Lake Manix, Mojave Desert, California, USA. Quaternary Research 83, 187–203. https://doi.org/10.1016/j.yqres.2014.11.003

Roberts, S.M., Spencer, R.J., 1995. Paleotemperatures preserved in fluid inclusions in halite. Geochimica et Cosmochimica Acta 59, 3929–3942. https://doi.org/10.1016/0016-7037(95)00253-V

Rupke, A.L., McDonald, A., 2012. Great Salt Lake brine chemistry database, 1966–2011. Utah Geological Survey, 596. Salt Lake City, UT, 1–7. https://ugspub.nr.utah.gov/publications/open_file_reports/ofr-596/ofr-596.pdf

Santi, L.M., Arnold, A.J., Ibarra, D.E., Whicker, C.A., Mering, J.A., Lomarda, R.B., Lora, J.M., Tripati, A., 2020. Clumped isotope constraints on changes in latest Pleistocene hydroclimate in the northwestern Great Basin: Lake Surprise, California. GSA Bulletin, 132, 2669–2683. https://doi.org/10.1130/B35484.1

Seager, R., Ting, M., Held, I., Kushnir, Y., Lu, J., Vecchi, G., Huang, H.P., Harnik, N., Leetmaa, A., Lau, N.C., Li, C., 2007. Model projections of an imminent transition to a more arid climate in southwestern North America. Science, 316, 1181–1184. https://doi.org/10.1126/science.1139601

Seager, R., Tzanova, A., Nakamura, J., 2009. Drought in the southeastern United States: Causes, variability over the last millennium, and the potential for future hydroclimate change. Journal of Climate, 22, 5021–5045. https://doi.org/10.1175/2009JCLI2683.1

Seltzer, A.M., Ng, J., Danskin, W.R., Kulongoski, J.T., Gannon, R.S., Stute, M., Severinghaus, J.P., 2019. Deglacial water-table decline in Southern California recorded by noble gas isotopes. Nature Communications 10, 5739. https://doi.org/10.1038/s41467-019-13693-2

Sirota, I., Enzel, Y., Lensky, N.G., 2017. Temperature seasonality control on modern halite layers in the Dead Sea: In situ observations. Geological Society of America Bulletin 129, 1181–1194. https://doi.org/10.1130/B31661.1

Smith, G.I., 1979. Subsurface stratigraphy and geochemistry of late Quaternary evaporites, Searles Lake, California. U.S. Geological Survey Professional Paper 1043, 130. https://doi.org/10.3133/pp1043

Smith, G.I., 2009. Late Cenozoic geology and lacustrine history of Searles Valley, Inyo and San Bernardino Counties, California. U.S. Geological Survey Professional Paper 128. https://pubs.usgs.gov/pp/1727/

Smoot, J.P., Lowenstein, T.K., 1991. Chapter 3 Depositional Environments of Non-Marine Evaporites, in: Melvin, J.L. (Ed.), Developments in Sedimentology. Elsevier, 50, 189–347. https://doi.org/10.1016/S0070-4571(08)70261-9

Stephens, D.W., 1990. Changes in lake levels, salinity and the biological community of Great Salt Lake (Utah, USA), 1847–1987. Hydrobiologia 197, 139–146. https://doi.org/10.1007/BF00026946

Stroup, J.S., Olson, K., Lowenstein, T.K., Jost, A.B., Mosher, H.M., Peaple, M.D., Feakins, S.J., Chen, C.Y., Lund, S.P., McGee, D., 2022. A >200 ka U-Th based chronology from lacustrine evaporites, Searles Lake, CA. Earth and Space Science Open Archive, 42. https://doi.org/10.1002/essoar.10512405.1

Wang, H., Liu, W., He, Y., Zhou, A., Zhao, H., Liu, H., Cao, Y., Hu, J., Meng, B., Jiang, J., Kolpakova, M., Krivonogov, S., Liu, Z., 2021. Salinity-controlled isomerization of lacustrine brGDGTs impacts the associated M B T 5 M E ' terrestrial temperature index. Geochimica et Cosmochimica Acta 305, 33–48. https://doi.org/10.1016/j.gca.2021.05.004

Woolfenden, W.B., 2003. A 180,000-year pollen record from Owens Lake, CA: terrestrial vegetation change on orbital scales. Quaternary Research 59, 430–444. https://doi.org/10.1016/S0033-5894(03)00033-4

FIGURE CAPTIONS

Figure 1. Study region and core records. (A) Regional map showing modern rivers and lakes/playas and the maximum extent of their pluvial counterparts during Marine Isotope Stage (MIS) 6. LVC = Long Valley Caldera. (B) Map of Searles Valley showing pluvial lake elevations and extent of modern salt pan. (C) Searles Lake subsurface stratigraphy from core KM-3 and nearby core SLAPP-SRLS17-1A/B. Lower Salt divided into salts (S1-7) and muds (M2-7). Modified from Smith (2009); Olson and Lowenstein (2021).

Figure 2. Environment, texture, and Searles Lake evaporite minerals as a function of brine concentration and temperature (modified from Olson and Lowenstein, 2021).

Figure 3. Elevation, depth and temperature from Great Salt Lake, Utah. Data collected and maintained by the Utah Department of Natural Resources, Utah Geological Survey (see Rupke and McDonald, 2012). (A) Historic lake elevation of Great Salt Lake; note the abrupt lake level rise starting in 1982. (B) Lake level and stratification. (C) Comparison of air temperatures with bottom water temperatures. (D) Inverse relationship between mean annual bottom water temperature range and mean annual lake depth. (E) Mean annual lake depth plotted against

706 bottom water temperature range. Data in (B)-(D) are from site AS2. See Figure S6 for GSL
707 sample locations.
708
709 **Figure 4.** Climate-lake relationships for non-tropic saline lakes. (A) Mean annual air temperature
710 (MAAT) versus mean annual bottom water temperature (MABWT) and (B) Annual bottom
711 water temperature (ABWT) range versus lake depth. Data point labels are salinity in g/L. Data
712 listed in Appendix A.
713
714 **Figure 5.** Comparison of Searles Lake temperature proxies. (A) Lithostratigraphy, (B) Evaporite
715 mineral stratigraphy, and (C) Brillouin and brGDGT temperatures from Searles Lake core
716 SLAPP-SRLS17-1A/B. Modeled evaporite facies temperature range (20–29 °C) of Olson and
717 Lowenstein (2021) shown with diagonal lines. Temperature thresholds (bottom arrows) from
718 Figure 2. Note the lack of natron and/or mirabilite in the evaporite stratigraphy. CAD =
719 Calcite/Aragonite/Dolomite, Gy = Gaylussite, Pr = Pirssonite, No = Northupite, Nh = Nahcolite,
720 Tr = Trona, Th = Thenardite, Bk = Burkeite, Ha = Halite, cmbs = composite meters below
721 surface.
722
723 **Figure 6.** Comparison of regional temperature records. (A) Searles Lake temperatures from
724 Brillouin thermometry and brGDGTs. (B) Groundwater noble gas temperatures from the Mojave
725 Desert (Kulongoski et al., 2009) and San Diego area (Seltzer et al., 2019). (C) Mean annual
726 temperature anamoly (± 2 SE) estimated by CRACKLE using plant macrofossil (packrat)
727 communities (Harbert and Nixon, 2018). (D) Juniper pollen from Owens Lake core OL-92
728 (Woolfenden, 2003). (E) Temperature record (± 2σ) from Lake Elsinore, California (Feakins et

al., 2019). Blue shading highlights the LGM (23–19 ka) and red shading highlight deglaciation (19–11 ka). See Figure S6 for locations of records discussed.

TABLE CAPTIONS

Table 1. Summary of Brillouin thermometry data for Searles Lake, California.

Table 2. Summary of Searles Lake Paleotemperatures.

736 **FIGURE 1 (Double Column)**

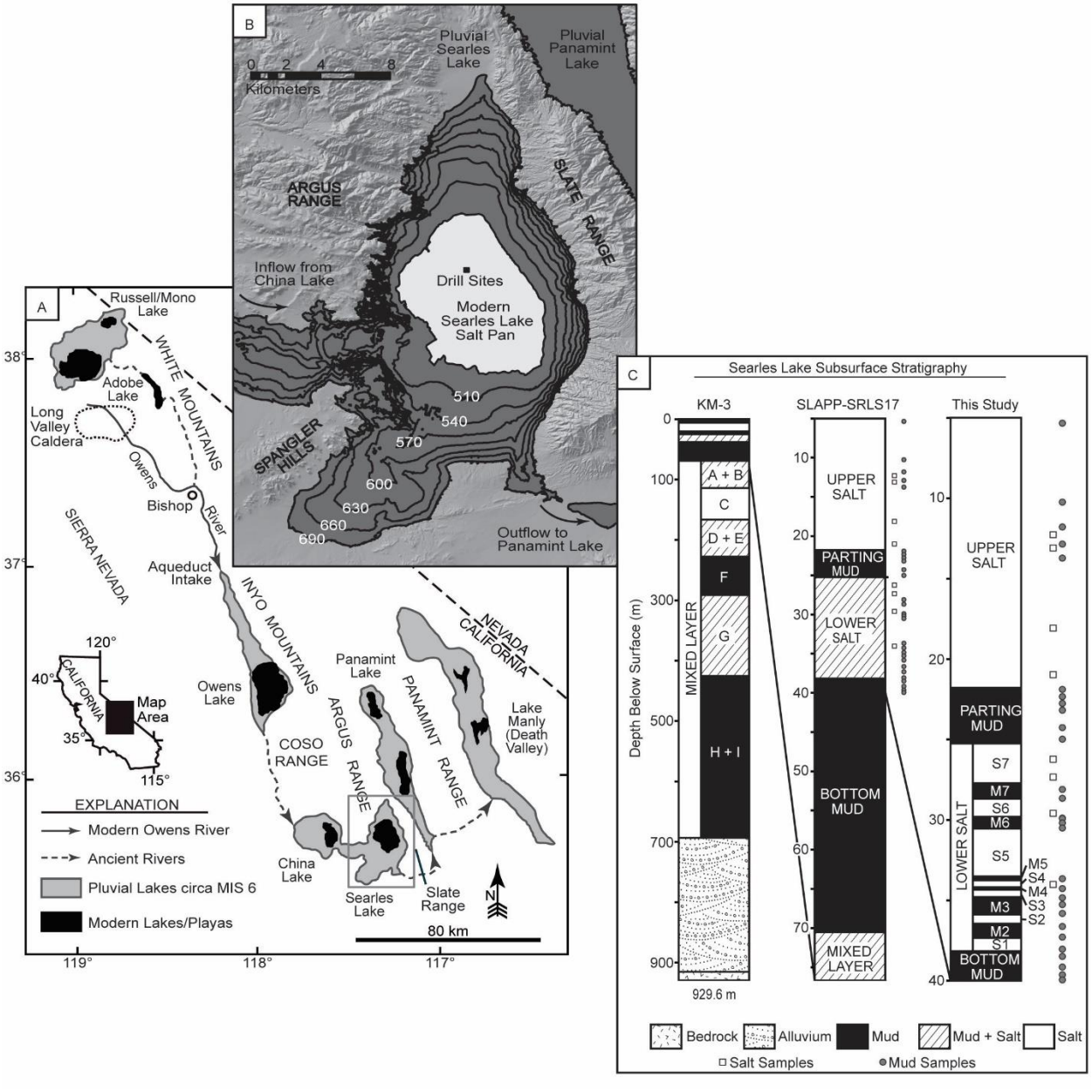

737

738

739 **FIGURE 2 (1.5 Column)**

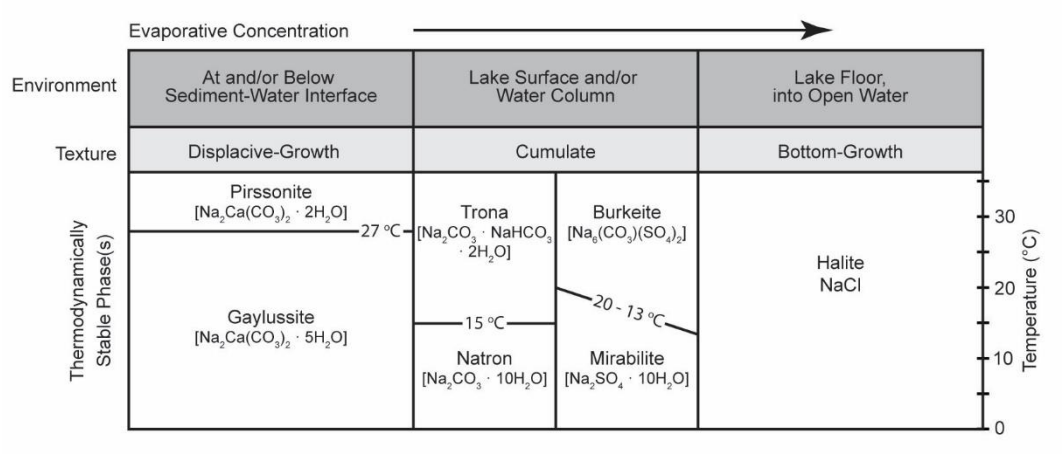

740

741

742

TABLE 1 (Double Column)

Stratigraphic Unit	Sample ID	Depth[*] (cmbs)	Age[†] (kya)	Population[§]	*n*	SD	Bottom Water Temperature (°C)		MSWD[**]	Maximum[††] Lake Depth (m)
							Mean	Range[#]		
Upper Salt	1A-6V 68–70 cm	12.27	8.5 ± 0.9	Crystal 1	8	2.2	21.6 ± 0.9			
				Crystal 2	8	0.9	21.1 ± 0.4			
				Crystal 3	5	1.2	26.8 ± 0.7			
				Average	3	2.3	22.4 ± 3.2	5.7 ± 0.8	30	10.4–19.0
	1A-7V 67–69 cm	13.09	9.0 ± 0.9	Crystal 1	4	1.8	17.1 ± 1.2			
				Crystal 2	6	1.8	22.1 ± 0.9			
				Crystal 3	9	2.2	18.3 ± 0.8			
				Average	3	2	19.4 ± 2.6	5.0 ± 1.5	7.5	10.6–19.4
	1A-10V 108–111 cm	18.08	12.1 ± 0.8	Crystal 1	8	1.9	23.9 ± 0.8			
				Crystal 2	5	2.5	18.3 ± 1.5			
				Crystal 3	8	2	19.8 ± 0.8			
				Average	3	2.2	21.4 ± 2.9	5.6 ± 1.7	11	10.4–19.1
	1B-7V 85–87 cm	20.97	14.0 ± 0.4	Crystal 1	10	1.9	22.6 ± 0.7			
				Crystal 2	4	1.5	22.7 ± 1.1			
				Crystal 3	7	2.3	21.7 ± 1.0			
Lower Salt				Average	3	0.4	22.4 ± 0.5	1.0 ± 1.5	0.31	NA
S7	1B-10V 104–106 cm	26.22	23.1 ± 0.5	Crystal 1	17	3.2	15.9 ± 0.8			
				Crystal 2	5	1.5	10.9 ± 0.8			
				Crystal 3	4	3.9	8.6 ± 2.7			
				Average	3	2.6	13.2 ± 3.6	7.3 ± 2.8	18	10.1–18.0
	1A-16V 131–133 cm	27.33	23.8 ± 0.5	Crystal 1	5	2.3	18.0 ± 1.3			
				Crystal 2	5	4.8	12.9 ± 2.7			
				Average	2	2	17.0 ± 3.6	5.1 ± 3.0	2.9	10.5–19.4
S6	1B-12V 139–141 cm	29.58	26.1 ± 0.9	Crystal 1	19	2.7	18.5 ± 0.7			
				Crystal 2	6	2.6	21.1 ± 1.3			
				Average	2	1.1	19.1 ± 1.8	2.6 ± 1.5	3.1	11.1–20.9
S4	1B-16V 25–27 cm	34.01	30.6 ± 1.0	Crystal 1	9	2.9	10.4 ± 1.1			
				Crystal 2	9	2.5	15.3 ± 1.0			
				Crystal 3	9	3.2	8.6 ± 1.2			
				Average	3	2.9	11.8 ± 3.6	6.7 ± 1.6	11	10.2–18.4

[*]cmbs = composite meters below surface.

[†]BACON age model based on U/Th geochronology. 2σ uncertainties. (Stroup et al., 2022).

[§]For Crystals, uncertainties given as standard error using a Student's t-distribution. Layer Averages are computed from the mean and SD of the two or three Crystals. Estimated uncertainty (SD) is biased weighted, temperature is weighted mean, and uncertainty (±) is unbiased weighted SD.

[#]BWT Range = Maximum Crystal temperature - Minimum Crystal temperature ± 1σ.

[**]Mean square weighted deviation.

[††]Computed from BWT Range using equations from Fig. 5E (lower estimate) and Fig. 6A (upper estimate).

743

744

FIGURE 3 (Single Column)

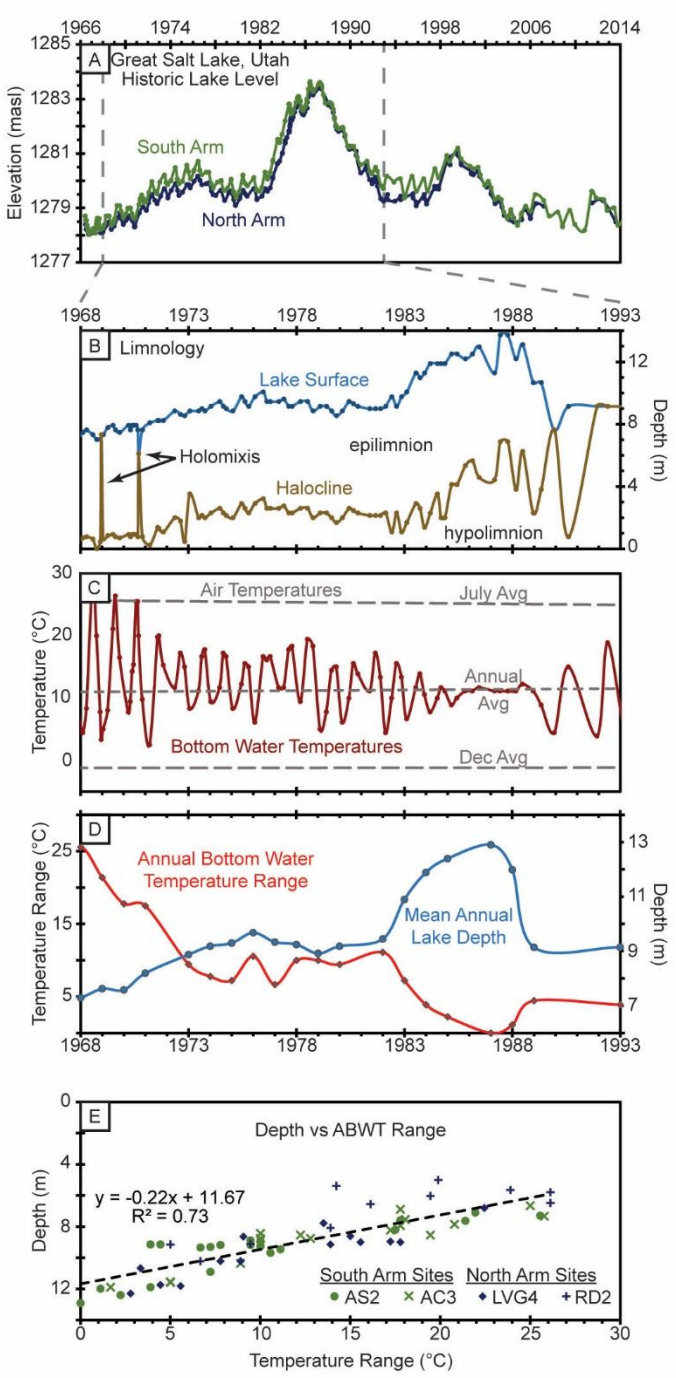

745

746

747 **FIGURE 4 (Double Column)**

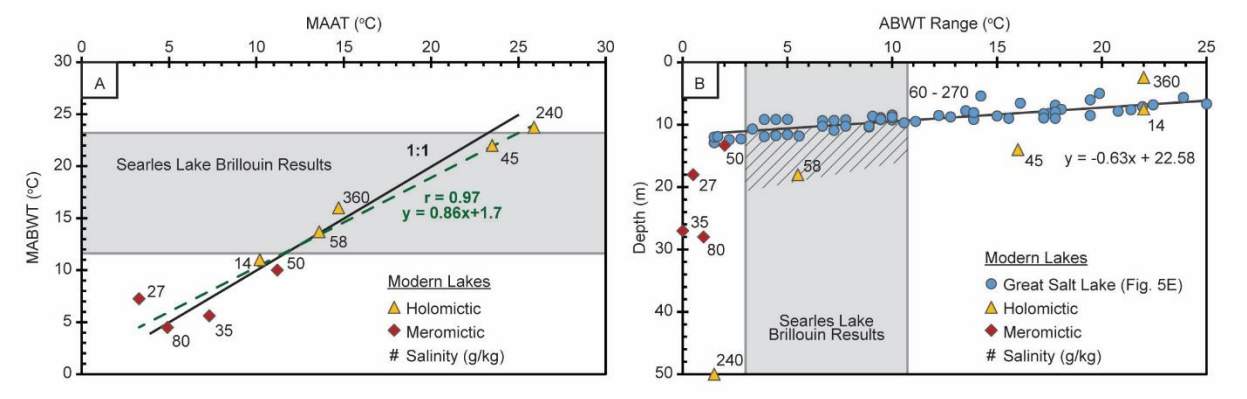

748

749

750

FIGURE 5 (1.5 Column)

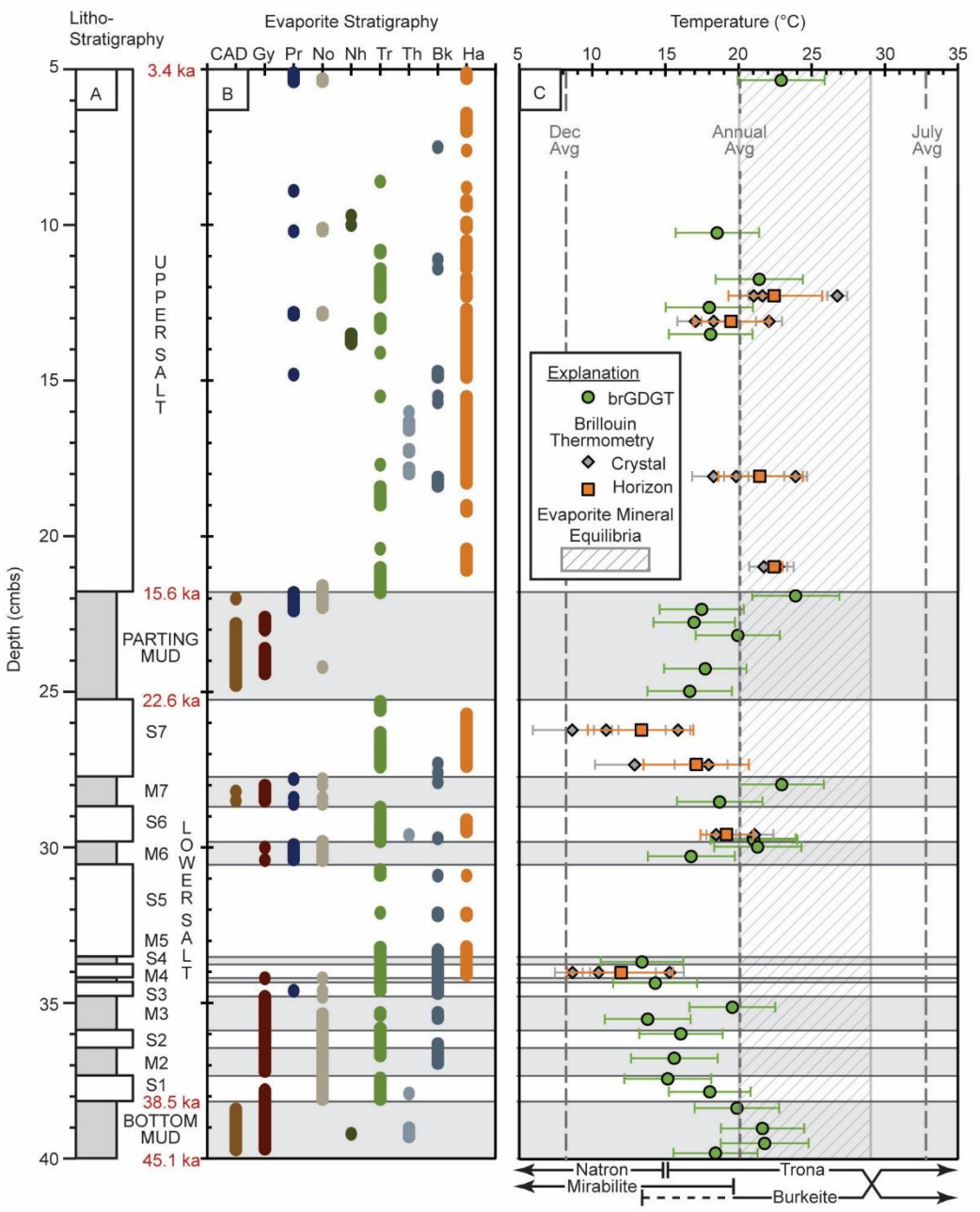

751

752

753 **TABLE 2 (Double Column)**

Interval	Age (kya)	*n*	Temperature (°C)*			
			Mean†	Min.#	Max.#	Range
Holocene	12-0	7	20.2 ± 2.1	18.0 ± 3.0	22.9 ± 3.0	4.9 ± 6.0
Last Glacial	45-14	28	17.9 ± 3.1	**11.8 ± 3.6**	23.9 ± 3.0	12.1 ± 6.6
MIS 1	14-0	9	20.4 ± 2.0	18.0 ± 3.0	22.9 ± 3.0	4.9 ± 6.0
MIS 2	29-14	15	18.8 ± 2.8	**13.2 ± 3.6**	23.9 ± 3.0	10.7 ± 6.6
MIS 3	45-29	13	16.8 ± 3.2	**11.8 ± 3.6**	21.8 ± 3.0	10.0 ± 6.6
Deglaciation	19-11	5	20.1 ± 3.1	17.0 ± 2.8	23.9 ± 3.0	6.9 ± 5.8
LGM	23-19	3	18.1 ± 1.7	16.7 ± 2.9	19.9 ± 2.9	3.3 ± 5.8
SLAPP-SRLS17	45-0	37	18.4 ± 3.1	**11.8 ± 3.6**	23.9 ± 3.0	12.1 ± 6.6

*1σ uncertainties.

†Weighted mean ± unbiased weighted SD.

#**Bold** values indicate Brillouin (salt) temperatures.

754

FIGURE 6 (Single Column)